AIAA JOURNAL
Vol. 48, No. 7, July 2010

Treatment of Nonmatched Grids for High-Accuracy Navier–Stokes Solutions

Boris Epstein*
Academic College of Tel-Aviv-Yaffo, 64044 Tel-Aviv, Israel
and
Sergey Peigin†
Israel Aircraft Industries, 70100 Ben-Gurion Airport, Israel

DOI: 10.2514/1.J050300

This paper handles the problem of accuracy loss for flow solutions on computational domains with a heterogeneous discretization on the subdomains. The problem occurs, e.g., when a composite multiblock mesh comprises blocks with different grid resolutions on the common boundary face. The problem is especially troublesome for high-accuracy solutions, in which tailoring of heterogeneous meshes frequently brings the loss of accuracy on a global scale. This paper focuses on the treatment of non-point-to-point structured multiblock grids, in which face-matched block boundaries are not necessarily point-matched. In the context of high-accuracy characteristic finite volume schemes for three-dimensional Navier–Stokes equations, a new approach is proposed that handles composite grids without the need in geometrical adjustment of boundary cells or any other grid-related preprocessing. In the proposed approach, interblock cell clusters are formed that contain boundary cells from the neighboring blocks of different resolutions. For each such cluster, the residuals of the Navier–Stokes equations are computed and then distributed among the cells of the host cluster by directly minimizing the flux imbalance in an appropriate norm. Outside these clusters, the residuals are computed in the regular way. The method allows automatic preservation of the conservative property of fluxes by placing constraints upon the optimum, it does not change the stability properties of the basic high-accuracy scheme and ensures a sufficiently high level of approximation on grids with reduced resolution. The results that include a number of numerical tests for two- and three-dimensional wings indicate good accuracy and robustness of the method and its applicability to full-scale Navier–Stokes computations.

Nomenclature

C_D	=	total drag coefficient
C_L	=	total lift coefficient
h_x, h_y, h_z	=	mesh size in x, y, z directions
M	=	freestream Mach number
R	=	residual
Re	=	freestream Reynolds number
x, y, z	=	Cartesian coordinates
u, v, w	=	velocity vector
α	=	angle of attack
λ	=	eigenvalue
σ	=	order of approximation

I. Introduction

THIS paper considers the problem of accuracy loss of Computational Fluid Dynamics (CFD) solutions on composite computational domains with a heterogeneous discretization within the subdomains. The problem occurs, e.g., when high-order numerical schemes are tailored with low-order schemes, or when the same order approximation is applied to blocks with different grid resolutions. The problem is especially troublesome for implementation of high-accuracy CFD solutions, since tailoring of heterogeneous discretizations frequently brings loss of accuracy not only locally, but on a global scale.

Received 19 October 2009; revision received 10 February 2010; accepted for publication 10 February 2010.

*Professor, School of Computer Sciences, 4 Antokolsky Street. Senior Member AIAA.

†Professor, Computational Fluid Dynamics Department, Engineering Division. Associate Fellow AIAA.

Specifically, we focus on the following case. Consider a structured multiblock computational grid around an aerodynamic configuration intended for the solution of full Navier–Stokes equations. Structured grids have important advantages that make them highly competitive for practical CFD. They may provide high-accuracy solutions without a need in complicated data structures (such as linked lists or graphs) for their implementation, which make them suitable for high-efficiency parallel computing [1]. Structured grids are also indispensable for CFD driven aerodynamic shape design, since they easily allow for fast and consistent grid movement.

Structured grids are conventionally constructed by means of Point-to-Point (PP) matched blocks. Unfortunately, the use of PP grids for complex aircraft configurations becomes problematic, due to the following reason. The nature of PP matching requires the propagation of the discrete topology of a block from aircraft surfaces to the outer boundaries of the grid (computational infinity). For complex aircraft configurations, the construction of such grids requires considerable human resources in terms of time and expertise. The regularity of the composite grid is frequently low, and the overall number of grid points becomes prohibitively high.

The above considerations brought a number of researchers, especially in industry, to the idea of using non-point-to-point (NPP) structured grids: that is, grids in which block boundaries are not necessarily point-matched [2–6]. NPP grids may significantly facilitate the use of structured grids, but the numerical implementation of the NPP approach appeared highly nontrivial, especially in the case of complicated geometries, due to the following reasons. First, in order to ensure the conservative property of numerical fluxes, it is necessary to tailor neighboring blocks with different cell partitions. This usually requires the exact adjustment of neighboring boundary block cells, located from both sides of the joint boundary, or another numerical or grid-generating procedure [7,8]. Both a direct adjustment of the boundary cells and alternative numerical procedures become sophisticated in the three-dimensional case. The second reason is associated with the implementation of high-accuracy characteristic numerical schemes, as in [1,9,10] in the case in which

the neighboring blocks possess different grid resolutions on the both sides of the joint boundary.

Within the framework of a time-iterated finite volume scheme of [9], in this work we propose a new approach to the problem of NPP. In the vicinity of each NPP interblock boundary, we form time-independent auxiliary clusters of minimum volume as follows:

1) Each cluster contains boundary cells from the neighboring blocks of different resolutions.

2) The cluster boundary is composed of cell faces that belong to only one of the neighboring blocks.

Thus, the original interblock boundary is swallowed by the cluster. In each time step, the residual computation is done in three stages. In the first stage, the residuals are calculated at the nonboundary (regular) numerical cells:, i.e., at the cells that do not belong to any of the above described clusters. Note that such cells constitute the vast majority of cells. The calculation is performed in a regular way as if the grid were of PP type: specifically, by means of the essentially-nonoscillatory (ENO) flux interpolating scheme (see [9] and Sec. II of the present paper). In these cells, no information across the block boundary is needed for the residual calculation, so the block localized numerical procedure is not affected by the distinction in grid partition between the neighboring blocks.

It is important that already in the course of the first stage, numerical fluxes are also determined at the outer boundary of the above clusters, since this boundary is composed of faces of the regular cells. In the second (collection) stage, the cluster residuals are computed. This is feasible, since the numerical fluxes at the cluster boundary are available from the first-stage computation stage as just explained in the previous paragraph. The overall cluster flux balance is thus composed of the fluxes at the cell faces that constitute the cluster boundary.

In the last, third (distribution), stage, the residuals at the irregular cells that belong to one of the clusters, are determined by algebraically minimizing the flux imbalance in an appropriate norm. Note that the optimization is performed for each cluster separately, and thus the number of optimization parameters is low. In a most simple mode of optimization, the least-squares method is applied while preserving the overall cluster flux balance. After the third stage, the residuals are available at all numerical cells of the composed grid, and the solution is advanced in time by the usual time integrating procedure.

The method allows bypassing the solution of nontrivial issues of characteristic interpolation across block faces with different left-side and right-side face partitions. This is done by avoiding the computation of the corresponding face fluxes that are swallowed by a boundary cluster. From the other side, the method allows automatically preserving the conservative property of the numerical scheme by placing simple constraints upon the optimization process. As a result, cell tailoring procedures usually typical of NPP schemes become redundant. The hybrid calculation of residuals did not change the stability properties of the basic ENO numerical scheme, and ensured sufficiently high level of accuracy on actually less resolved grids. The time expenditure for the residual handling at irregular cells (stages 2 and 3) appeared negligible and did not harm the high parallelization efficiency of the method. The results, which include a number of numerical tests for two- and three-dimensional wings indicate accuracy and robustness of the method and its applicability to full-scale Navier–Stokes computations in an engineering environment.

II. Preliminary Considerations

A. Basic Numerical Approach

A finite volume numerical ENO scheme developed in [9,10] for the solution of steady-state Navier–Stokes equations was originally applied on point-to-point-matched structured multiblock grids. In Cartesian coordinates the continuous equations take the form

$$\frac{\partial \mathbf{q}}{\partial t} + \mathrm{div}\mathbf{C} = \mathrm{div}\mathbf{V} \tag{1}$$

where the tensor $\mathbf{C} = (\mathbf{f}, \mathbf{g}, \mathbf{h})$ represents the convection terms, the tensor $\mathbf{V} = (\mathbf{r}, \mathbf{s}, \mathbf{t})$ represents the viscous terms, $\mathbf{q} = (\rho, \rho u, \rho v, \rho w, E)$, ρ is the density, (u, v, w) is the velocity vector, E is the energy, t is the time, $\mathbf{f}$, $\mathbf{g}$, $\mathbf{h}$ are the inviscid (convection) fluxes and $\mathbf{r}$, $\mathbf{s}$, $\mathbf{t}$ are the viscous fluxes that depend in a nonlinear mode on $\mathbf{q}$ (for more detail, see [11]).

The assumption of PP matched structured blocks means that the grid consists of a number of blocks, where each block has (i, j, k) structure and that interblock boundaries are point-to-point-matched (see Fig. 1). Integrating over each cell separately in a finite volume manner, we get a system of ODEs that can be solved by a time-stepping procedure. For particular cell (i, j, k) the following approximation is assumed:

$$\begin{aligned}
&(\Omega_{i,j,k}\mathbf{q}_{i,j,k})_t + [\mathbf{C}\cdot(S\mathbf{n})]_{i+1/2,j,k} - [\mathbf{C}\cdot(S\mathbf{n})]_{i-1/2,j,k} \\
&\quad + [\mathbf{C}\cdot(S\mathbf{n})]_{i,j+1/2,k} - [\mathbf{C}\cdot(S\mathbf{n})]_{i,j-1/2,k} + [\mathbf{C}\cdot(S\mathbf{n})]_{i,j,k+1/2} \\
&\quad - [\mathbf{C}\cdot(S\mathbf{n})]_{i,j,k-1/2} - [\mathbf{C}\cdot(S\mathbf{n})]_{i,j-1/2,k} + [\mathbf{C}\cdot(S\mathbf{n})]_{i,j,k+1/2} \\
&\quad - [\mathbf{C}\cdot(S\mathbf{n})]_{i,j,k-1/2} = [\mathbf{V}\cdot(S\mathbf{n})]_{i+1/2,j,k} - [\mathbf{V}\cdot(S\mathbf{n})]_{i-1/2,j,k} \\
&\quad + [\mathbf{V}\cdot(S\mathbf{n})]_{i,j+1/2,k} - [\mathbf{V}\cdot(S\mathbf{n})]_{i,j-1/2,k} + [\mathbf{V}\cdot(S\mathbf{n})]_{i,j,k+1/2} \\
&\quad - [\mathbf{V}\cdot(S\mathbf{n})]_{i,j,k-1/2}
\end{aligned} \tag{2}$$

where $\Omega_{i,j,k}$ is the cell volume, $\mathbf{q}_{i,j,k}$ in some mean value of $\mathbf{q}$ over the cell and S is the area of a cell side surface.

Fluxes with half-indices are approximated by a one-dimensional interpolation from the near-by cell centers, based on the ENO concept [12] with a specific flux interpolation technique close to that of [13]. More details may be found in [9,14]. Nonlinear stability is maintained via approximation of inviscid fluxes on a variable template according to local characteristics and smoothness of the fluxes; viscous fluxes are approximated in a straightforward way. An ENO interpolation template (typically consisting of three points on the finest multigrid level) is determined separately for each characteristic field, primarily according to the sign of the corresponding eigenvalue, and then according to the smoothness of fluxes.

In the framework of the method, the above ENO procedure is applied only for the defect correction calculation, a very limited number of times (roughly equal to the number of multigrid cycles), and most of the computational work is performed using a relatively inexpensive upwind-biased relaxation. Time-marching is performed by a three-stage Runge–Kutta scheme used in a total-variation-diminishing (TVD) form [13]. Note that the conservative property of the original PP-oriented scheme was achieved through the transparency of interblock boundaries in such a way that the interpolation template might include the cell values across the block boundary.

B. Discussion of the Problem

In this work we aim to extend the above numerical scheme of [9,10] to NPP meshes. In this case, numerous problems arise even within of low-order numerical schemes or incompressible flows [15]. Within a more demanding framework of high-order characteristic schemes on NPP grids, the following interrelated numerical drawbacks must be overcome: loss of accuracy, deterioration of stability, and violation of conservative property. To illustrate this consider a fragment of a heavily simplified model two-dimensional NPP grid depicted in Fig. 2, in which block 2 possesses a twice-higher partition in the y direction than in block 1 while keeping the same as in block 1 partition in the x direction,

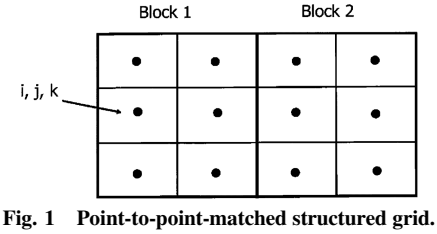

Fig. 1 Point-to-point-matched structured grid.

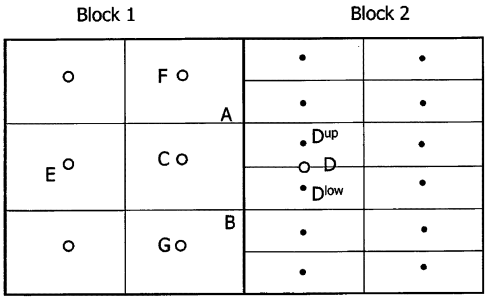

Fig. 2 Non-point-to-point-matched structured grid.

First, consider the Poisson equation that models viscous terms in full Navier–Stokes equations. Looking for the finite volume solution on the grid of Fig. 2, we must approximate the term $u_x \cdot |AB|$, which is the numerical flux at face AB, located at the boundary between block 1 and block 2. A natural approximation for this is the finite difference $(u_D - u_C)/h_x$. Since block 2 is twice finer in y direction it does not provide the value of u at point D but instead two values above and below D, D^{up} and D^{low}, are available.

The linear interpolation based on these values yields the following approximation:

$$u_x = \frac{0.5(u_D^{\text{up}} + u_D^{\text{low}}) - u_C}{h_x}$$

This means that the order of approximation of Poisson equation at point C is

$$\frac{u_E - 2u_C + 0.5(u_D^{\text{up}} + u_D^{\text{low}})}{h_x^2} + \frac{u_F - 2u_C + u_G}{h_y^2} = \mathcal{O}(h_x^2 + h_y^2) + \mathcal{O}\left(\frac{h_y^2}{h_x^2}\right) \tag{3}$$

It is possible to improve the order of approximation by enlarging the computational template in the x direction or by significantly increasing the order of interpolation in the y direction. For example, approximating the value at point D up to $\mathcal{O}(h_y^4)$ will yield $\mathcal{O}(h_y^4/h_x^2)$ in the last term of Eq. (3). Note that in the both cases, the approximation to the equation is not even consistent when $h_y \gg h_x$.

Now consider the approximation of convective terms of Eq. (1) on the grid of Fig. 2. Similar to the approximation of viscous terms, the needed solution value at this point is interpolated using actually existing grid points D^{up} and D^{low} of block 2. Similar to relation (3), the straightforward interpolation yields the order of approximation $\mathcal{O}(h_y^2/h_x)$, which is again prohibitive when $h_y \gg h_x$. As the order of noncharacteristic interpolation increases, prompted by the requirement of accurate approximation, the enhancement of stability becomes even more conjectural.

The third problem is that of preserving the conservative property of the numerical scheme. For example, a flux at face AB calculated at cell C must be equal to the sum of the corresponding face fluxes calculated at cells D^{up} and D^{low}. This requires not only the full geometrical conformity of the boundary cell faces from the both sides of the interblock boundary, but also the exact adjustment of the corresponding numerical fluxes. Since the numerical procedure of [10,13] performs flux interpolation in the characteristic fields, the adjustment of numerical fluxes implies the adjustment of the corresponding eigenvalues on the both sides of the boundary. These are non trivial requirements even for a simple grid of Fig. 2. For curvilinear three-dimensional NPP structured blocks with arbitrary partition, this becomes almost infeasible.

III. New Approach

Based on the considerations of the previous section we observe that the approximation of NPP block boundary fluxes is troublesome in terms of accuracy and stability. This may lead to intractable problems and seriously flaw the use of NPP structured grids. On the other hand, the problem is confined to narrow strips in the vicinity of NPP block boundaries. This gives rise to the following idea. Block boundary fluxes are only needed in order to determine residuals in the bordeline cells. These residuals may be computed through an alternative numeric procedure different from the basic ENO technique. Both numerical procedures must be of course compatible in order to ensure the conservative property of the resulting composite scheme.

Before describing the new procedure in detail, the following remark may be made. In principle, it is possible to numerically solve the boundary-value problem for a partial differential equation by directly minimizing the residuals of a discrete approximation in an appropriate norm. Some attempts in this direction have been made in the recent years in the field of CFD (see [16]). So far, these attempts were confined to low-accuracy gas-dynamic models on relatively coarse grids. In our opinion, the reason for this lies in the fact that optimization methods become highly inefficient when high-dimensional search spaces are needed, which is the case in which Euler or Navier–Stokes equations are to be solved. For a relatively simple geometry of three-dimensional aerodynamic wing, the number of optimization parameters (flowfield variables) may reach several hundred thousands or even one million, which makes existing optimization methods practically nonapplicable.

The situation changes when a direct residual minimization is restricted to a small subdomain of the computational grid such as interblock strips or their subsets. In this case the number of optimization parameters is relatively low, which makes the optimization practically feasible. On the other hand, the compatibility of the optimization procedure with the characteristic flux determination on the boundary of the subdomain, does not allow for sawtooth solutions.

The proposed algorithm for residual determination in the boundary interblock strips includes several stages. In the preliminary (preprocessing) stage, time-independent auxiliary cell clusters are formed. Each such cluster comprises cells of the existing grid taken from the neighboring blocks of different partitions in such a way that the following two properties are fulfilled:

1) The cluster boundary is composed of cell faces that do not belong to the interblock boundary.

2) Each cluster represents a minimum volume set; that is, its own cell subclusters do not satisfy property 1.

For example, in Fig. 2, cells C (block 1), D^{up}, and D^{low} (block 2) constitute such a cluster, since the boundary of the cluster includes three faces of cell C (west, north and south), two faces of cell D^{up} (north and east), and two faces of cell D^{low} (south and east), each belonging to only one of the two blocks, and any cell deletion from this cluster will destroy the single-citizenship property 1. Finally, the above cluster definitions imply that the original interblock boundary is swallowed by the cluster. For example, in Fig. 2, face AB became internal to the cluster $\{C, D^{\text{up}}, D^{\text{low}}\}$.

The preprocessing stage performs the minimal cluster coverage of grid cells with a face that belongs to two neighboring blocks, which possess a different resolution in a direction tangential to the interblock boundary surface.

At each iteration, the computation of residuals is divided into three stages. In the first stage of the numerical procedure, the residuals are determined in the regular cells: that is, cells that do not belong to any of the clusters. The calculation is performed by means of the regular ENO flux interpolating scheme described in Sec. II.A. This calculation is feasible, since in the regular cells, it is possible to perform characteristic flux interpolation without necessarily using the information from the other side of the interblock boundary. For example, in terms of Fig. 2, the flux at the west face of cell C has at hand not only the solution values at cell centers to the west of the face but also the solution value at the cell-center C.

A proper ENO-style choice of template from available cell centers ensures the stability of the numerical scheme. Thus, we avoid the difficulties related to the flux computation on the interblock boundary, since the corresponding fluxes are swallowed by the cluster. Note that the original stable characteristic computation of the boundary fluxes might require values at the cell centers across the boundary.

In fact, the proposed bypasses the problematic issues related to the tailoring of blocks with different partitions on the common boundary. The exact position of the interblock cell faces is of little relevance, since they are swallowed by interblock clusters. Additionally, the flux values on the faces are not determined by the usual characteristic algorithm, but are instead determined implicitly by the minimization of the corresponding residuals (flux balances).

Of course, regular cells constitute the vast majority of grid cells. Note that in the course of the first stage, the numerical fluxes have been determined at all boundaries of the clusters, since these boundaries are formed by faces of the regular cells. This allows performing the second stage of the numerical procedure: the collection stage, in which cluster residuals are determined. More exactly, the overall flux balance of a cluster is composed of the fluxes at the faces of the cluster boundary. As just explained above, the fluxes at the cluster boundary have been calculated in the first (regular) stage, since they also belong to the regular cells.

In the third (distribution) stage, it is necessary to distribute the cluster residuals among the cells that make it up. Since the cell flux balance represents (within a factor of volume) the residual of the steady-state equation, the minimization of cell residuals is equivalent to the minimization of cell flux balances in an appropriate norm. This is performed algebraically subject to the following constraints:

1) The overall cluster flux balances are equal to those computed at the collection stage.

2) The flux conservative property of the numerical scheme is preserved.

The last property is satisfied by placing simple constraints upon the optimization procedure. Figure 2 illustrates this for a simplified grid. In this model case, we require the fulfilment of the following relation (FB stands for flux balance):

$$\mathrm{FB}\,(D^{\mathrm{up}}) + \mathrm{FB}(D^{\mathrm{low}}) + \mathrm{FB}(C) = \mathrm{FB}(\mathrm{cluster}(C, D^{\mathrm{up}}, D^{\mathrm{low}})) \quad (4)$$

where $\mathrm{cluster}(C, D^{\mathrm{up}}, D^{\mathrm{low}})$ is defined, as explained above, by the north, south, and west faces of cell C; north and east faces of D^{up}; and south and east faces of D^{low}.

If the least-squares minimization is applied with the relation (4) used as a constraint, the whole procedure yields

$$\mathrm{FB}\,(D^{\mathrm{up}}) = \mathrm{FB}(D^{\mathrm{low}}) = \tfrac{1}{2}\mathrm{FB}(C) = \tfrac{1}{4}\mathrm{FB}(\mathrm{cluster}(C, D^{\mathrm{up}}, D^{\mathrm{low}})) \quad (5)$$

This follows from the fact, that under the constraint $R_1 + R_2 = R$, the expression $R_1^2 + R_2^2$ achieves its minimum with $R_1 = R_2 = R/2$.

The optimization proceeds separately for each cluster that keeps the number of optimization parameters to a low level. After the third stage, the residuals are determined in all the grid cells, which allows advancing the solution by the usual time-stepping scheme of Sec. II.A. Going back to the Poisson equation, a simple check shows that the new procedure ensures (contrary to the naive scheme) the order of approximation $\mathcal{O}(h_x^2 + h_y^2)$.

Since the conservative property of the scheme is thus ensured automatically, typical NPP tailoring procedures become redundant. The whole approach allows hybridizing nonadjusted neighboring blocks in an a posteriori manner. It appeared that the hybrid residual calculation procedure does not have an adverse effect on the stability of the original ENO numerical scheme, and the time expenditure for the treatment of irregular cells is negligible, which allows retaining the high parallel efficiency of the method.

IV. Resulting Numerical Scheme: Stability Considerations and Consistency Conditions

A. Generic Model Problem

Consider the numerical scheme stemming from the proposed approach for several simple but representative model problems. With this end in view, we introduce a one-dimensional grid consisting of cells of length h:

$$x_i = h \cdot (i - 1/2)$$

where cell centers correspond to $i = 1, 2, 3, \ldots$ and cell boundaries are set at $i = 1/2, 3/2, 5/2, \ldots$. We are interested in the steady-state solution u of the boundary-value problem for a generic equation:

$$\frac{\partial u}{\partial t} + \frac{\partial f}{\partial x} = 0 \quad (6)$$

In the following, we consider the hyperbolic case in which $f = f(u)$ and the case of a mixed equation:

$$\frac{\partial u}{\partial t} + c\frac{\partial u}{\partial x} - \nu\frac{\partial^2 u}{\partial x^2} = 0 \quad (7)$$

which corresponds to $f = cu - \nu u_x$.

The model equation is solved by a finite volume numerical scheme

$$\frac{\partial u_i}{\partial t} + \frac{f_{i+1/2} - f_{i-1/2}}{h} = 0 \quad (8)$$

starting from an initial guess

$$u^\circ = u(0, x) \quad (9)$$

with addition of appropriate boundary conditions.

To model the proposed approach, we assume that the cell boundary at $i = k + 1/2$ represents a non-point-to-point face; that, is the flux value at this face cannot be computed by the regular way (through the values at the neighboring cell centers) and is instead subject to the NPP procedure described previously in Sec. III. Our aim is to check the influence of the changes thus introduced into the numerical scheme, on its approximation and stability properties, and to formulate consistency conditions.

B. Nonlinear Conservation Law

Consider a case of the steady-state solution for a nonlinear Eq. (6): that is, when $f = f(u)$ depends nonlinearly on u. A good example for this is Burgers's equation,

$$f = \tfrac{1}{2}u^2, \qquad u(0) = 1, \qquad u(1) = -1$$

solved on the grid of Sec. IV.A with a nonmatched grid singularity at $x = x_k$.

At regular points ($i \neq k + 1/2$), consider a simple upwind flux approximation with entropy fix:

$$\begin{aligned}
&f_{i+1/2} = f_i, \qquad \text{if } f'(u_i) > 0, \qquad f'(u_{i+1}) > 0\\
&f_{i+1/2} = f_{i+1}, \qquad \text{if } f'(u_i) < 0, \qquad f'(u_{i+1}) < 0\\
&f_{i+1/2} = \frac{1}{2}(f^+_{i+1/2} + f^-_{i-1/2}), \qquad f^+_{i+1/2} = f_i + \lambda u_i\\
&f^-_{i+1/2} = f_{i+1} - \lambda u_{i+1}, \qquad \lambda = \max\{|f'(u_i)|, |f'(u_{i+1})|\}
\end{aligned} \quad (10)$$

in the remaining cases. At $i = k + 1/2$ (NPP face), a modified scheme of Sec. III is applied.

A thorough analysis demonstrates that the scheme retains its TVD properties provided the following conditions are met:

1) If the sign of $f'(u)$ changes exactly across the nonmatched face $i = k + 1/2$, the entropy-fix procedure is applied at both faces $k - 1/2$ and $k + 3/2$.

2) The corresponding values of λ are chosen as

$$\lambda = \max\{|f'(u_{k-1})|, |f'(u_k)|, |f'(u_{k+1})|, |f'(u_{k+2})|\}$$

C. Model Linearized Navier–Stokes Equation

Finally, we consider the following model equation:

$$\frac{\partial u}{\partial t} + c\frac{\partial u}{\partial x} - \nu\frac{\partial^2 u}{\partial x^2} = 0, \qquad u(t = 0, x) = u^\circ(x) \quad (11)$$

which corresponds to Eq. (6) with $f = cu - \nu u_x$.

Table 1 Point-to-point NES vs OVERFLOW computations of drag values at $M = 0.76$ and $C_L = 0.5$ in aerodynamic counts

Geometry	NES C_D^{visc}	NES C_D^{pres}	NES C_D	OVERFLOW C_D^{visc}	OVERFLOW C_D^{pres}	OVERFLOW C_D
DPW-W1	57.3	160.5	217.8	59.3	160.0	219.3
Case o3	58.4	142.4	200.7	60.7	140.6	201.3
Case o4	58.3	145.9	204.3	60.7	143.8	204.5
Case o5	58.2	145.4	203.6	60.7	142.5	203.2

We assume the following boundary conditions:

$$cu(0) - \nu u_x(0) = a, \qquad u(1) = b \tag{12}$$

Here, a finite volume semidiscrete scheme (8) and (9) is applied on the grid described in Sec. IV.A. We are looking for the steady-state solution and assume that the time-marching is performed explicitly using the current residuals of the space discretization. Again, we assume that the cell boundary at $i = k + 1/2$ models a non-point-to-point face, and the flux at this face is computed through the procedure of Sec. III. At the regular faces we assume the following approximation (upwind in respect to the convection term):

$$f_{i+1/2} = cu_i - \nu \frac{u_{i+1} - u_i}{h} \tag{13}$$

At every regular point (that is, at $i \neq k,\ k+1$) the residual is computed by using Eq. (13). At points k and $k+1$, the procedure of Sec. III yields residuals R_1 and R_2, subject to optimization under the constraint

$$R_1 + R_2 = c\frac{u_{k+1} - u_{k-1}}{h} - \nu \frac{u_{k+2} - u_{k+1} - u_k + u_{k-1}}{h^2} \tag{14}$$

Consider the trivial optimization $R_1 = R_2$. Then, in the steady-state ($\partial u/\partial t = 0$), the assumed discretization yields a matrix with two identical rows that correspond to $i = k$ and $i = k+1$, which indicates that the solution depends on a free parameter. In fact, since we assumed

$$\frac{\partial u_k}{\partial t} = \frac{\partial u_{k+1}}{\partial t}$$

then this parameter is $u_k - u_{k+1} = u_k^\circ - u_{k+1}^\circ \equiv \epsilon$. Finally, this means that the solution of Eqs. (11–14) depends on the value of ϵ.

We are going to estimate the propagation of the noise ϵ. Assuming the homogeneous boundary conditions $a = b = 0$ it is possible to write down the exact discrete steady-state solution of Eqs. (11–14) in the following form:

$$u_i = 0 \quad (\text{for } i \geq k+1); \qquad u_i = \frac{\epsilon}{(1 + ch/\nu)^{k-i}} \quad (\text{for } i \leq k) \tag{15}$$

We see that the noise exponentially decays in the upwind direction, provided the ratio ch/ν is sufficiently high.

The whole problem can be avoided by setting $\epsilon = 0$. The condition $\epsilon = 0$ yields $u_k = u_{k+1}$, which introduces a local approximation error. It is interesting to estimate how this error propagates inside the NPP blocks. With this end in view, consider Eq. (11) with a nonzero right-hand side:

$$\frac{\partial u}{\partial t} + c\frac{\partial u}{\partial x} - \nu \frac{\partial^2 u}{\partial x^2} = c, \qquad u(t = 0, x) = x \tag{16}$$

$$cu(0) - \nu u_x(0) = -\nu, \qquad u(1) = 1 \tag{17}$$

which, in the continuous case, is equivalent to Eqs. (11) and (12) with $a = b = u^\circ(x) = 0$ after the substitution $u^{\text{new}} = u + x$.

The exact solution of Eqs. (16) and (17) is $u = x$, which, of course, corresponds to the trivial solution $u = 0$ for Eqs. (11) and (12) with $a = b = u^\circ(x) = 0$. In the discrete case, the conditions in Eqs. (16) and (17) do not allow exactly reproducing the continuous solution

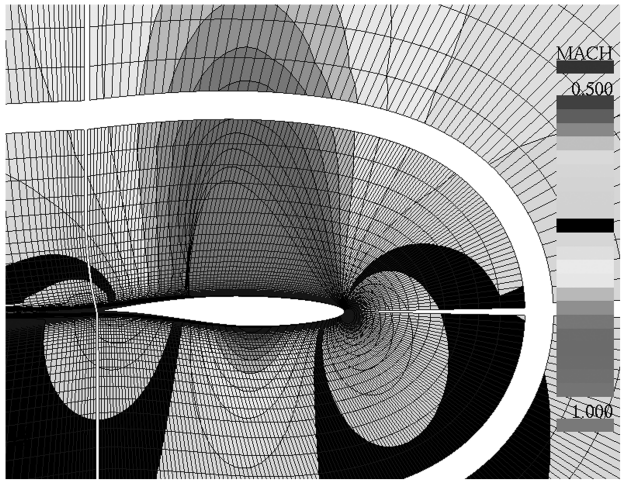

Fig. 4 Case P3, NPP ratio 128:64, and iso-Mach contours at $\alpha = 1.5°$ and $M = 0.75$.

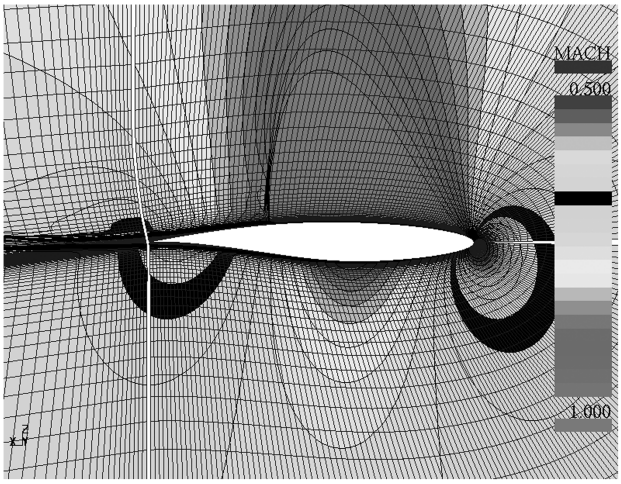

Fig. 3 Case P1, NPP ratio 128:48, and iso-Mach contours at $\alpha = 1.5°$, $M = 0.75$.

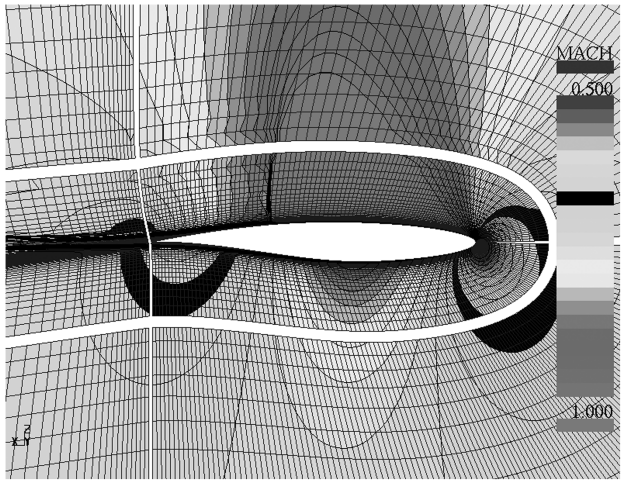

Fig. 5 Case P4, NPP ratio 128:64, and iso-Mach contours at $\alpha = 1.5°$ and $M = 0.75$.

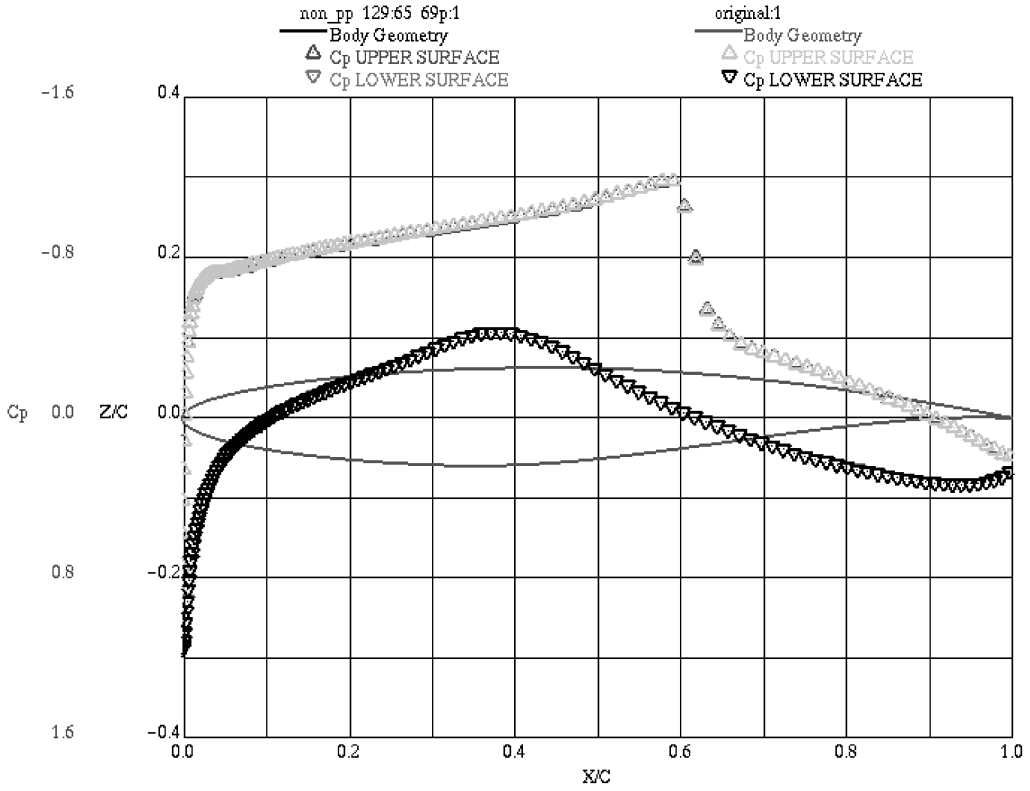

Fig. 6 Case P3, NPP ratio 128:64, and C_P distribution at $\alpha = 1.5°$ and $M = 0.75$.

$u = x$, where the initial NPP condition $u_k^\circ = u_{k+1}^\circ$ is applied. Since, with $u_k^\circ = u_{k+1}^\circ$, u_k stays equal to u_{k+1} at every time step, the steady-state discrete solution necessarily contains numerical noise that is to be estimated now.

Similar to the case in the first part of the present section, we may write down the exact solution of the NPP discretization of Eqs. (16) and (17):

$$u_i = x_i = h \cdot (i - 1/2) \quad (\text{for } i \geq k+1)$$
$$u_i = x_i + h \cdot \theta^{k-i} \quad (\text{for } i \leq k) \tag{18}$$

where $\theta = (1 + ch/\nu)^{-1}$.

The check shows that the scheme is exactly satisfied for all values of i, including the nonmatched cells $i = k$ and $i = k + 1$. Thus, the approximation error yielded by the consistency condition $u_k^\circ = u_{k+1}^\circ$,

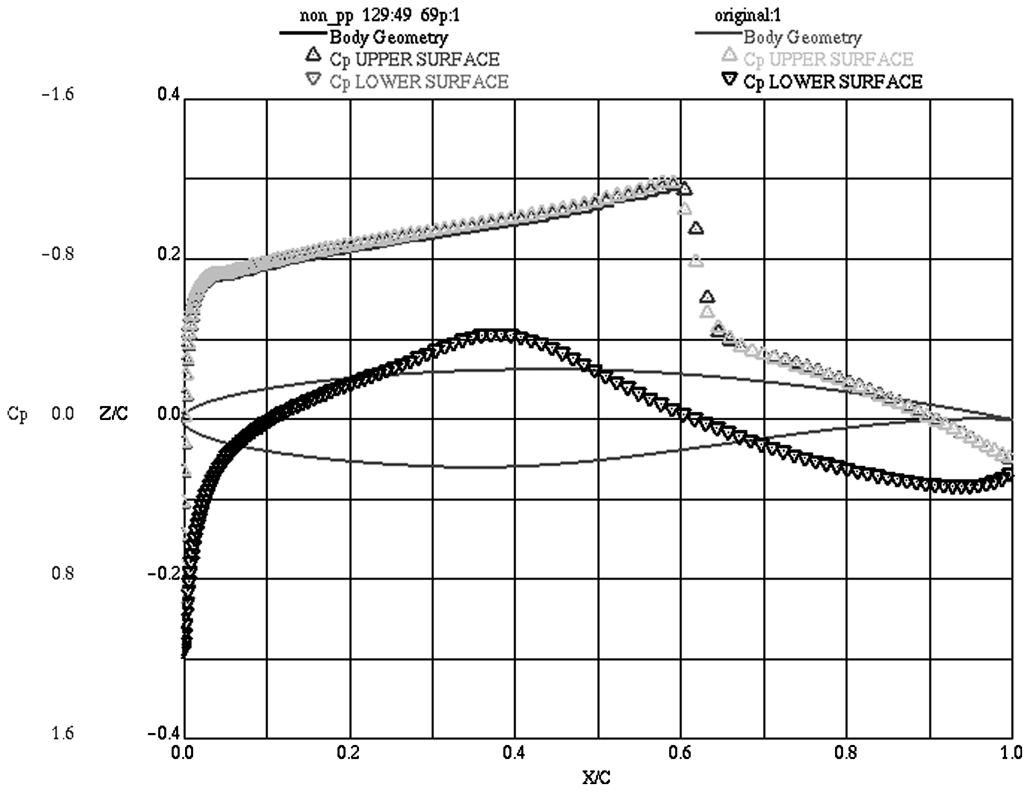

Fig. 7 Case P3, NPP ratio 128:48 and C_P distribution at $\alpha = 1.5°$ and $M = 0.75$.

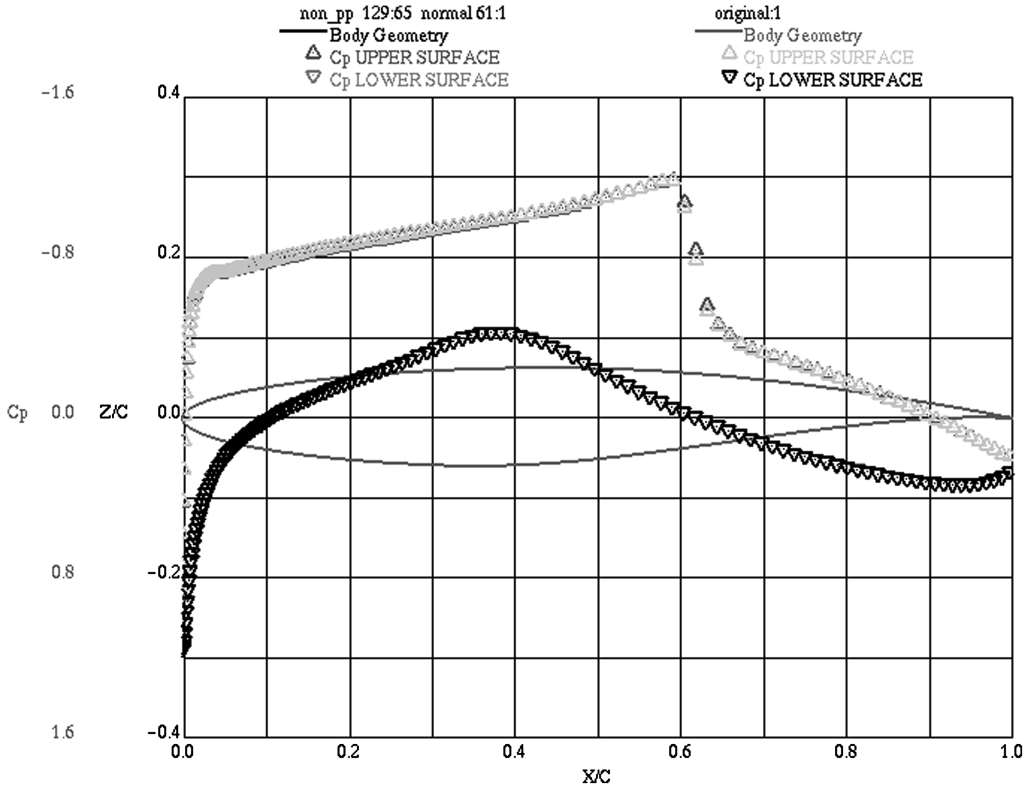

Fig. 8 Case P4, NPP ratio 128:64 and C_P distribution at $\alpha = 1.5°$ and $M = 0.75$.

decays exponentially in the upwind direction with the decay speed $1 + ch/\nu$ per grid cell.

V. Results and Discussion

Before performing the verification study for the NPP approach, let us consider the systematic comparison between the original solver NES (based on point-to-point meshes) and the NASA code OVERFLOW [17]. The corresponding comparison (flow simulation over four different 3-D wings at $M = 0.76$, $C_L = 0.5$) is given in Table 1 for the values of viscous drag C_D^{visc}, pressure drag C_D^{pres} and total drag C_D computed by the code NES and the code OVERFLOW. More details may be found in [18]. It may be concluded, that the two codes yield very similar drag results in terms of both viscous and pressure drag for a wide range of tested geometries. Specifically, on the average the difference between C_D values by these two codes is about 1 count.

Based on the present approach for treatment of NPP grids, a new industrial code for solution of full Navier–Stokes equations on non-point-to-point meshes, has been developed. The new code features the automatic recognition of NPP boundaries with no restriction on the i, j, and k orientation of the blocks.

To verify the proposed new approach, the above procedure was applied to the computation of the flow over RAE2822 airfoil at transonic conditions ($M = 0.75$). The original point-to-point-matched grid comprised four blocks: upper airfoil, lower airfoil (with dimensions $i_{\max} = 128$ and $j_{\max} = 96$ in the streamwise and normal directions, respectively), upper wake, and lower wake (with the corresponding dimensions $i_{\max} = 64$ and $j_{\max} = 96$).

For the verification studies, the upper airfoil block was subdivided into two subblocks along the grid line $j = J^* = \text{const}$. A total of four test cases were considered (labeled case P1 to case P4) for different values of the above constant. The dimensions of the first subblock (near the airfoil) were kept to the original level ($i_{\max} = 128$, $j_{\max} = J^*$), whereas the i dimension of the second subblock was significantly reduced (from the original 128 to 64 and 48). The location of the cut line was varied in the wide range: from a remote position (with respect to the airfoil) case P1 to a very close position

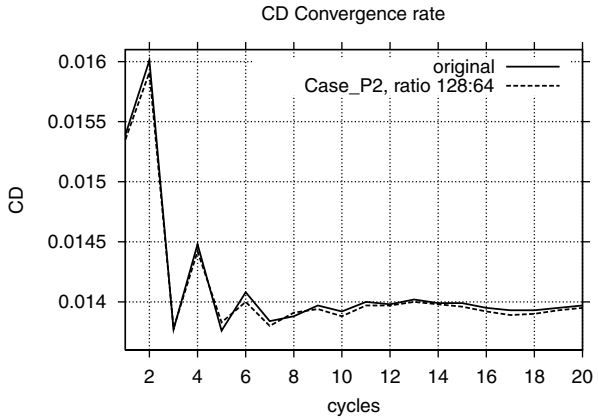

Fig. 9 Case P2, NPP ratio 128:64. Convergence of C_D at $\alpha = 1.5°$ abd $M = 0.75$.

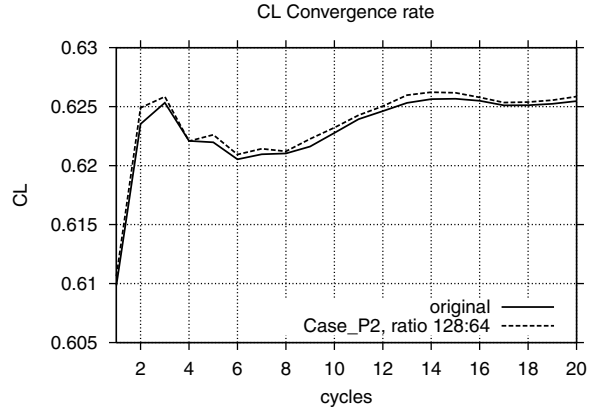

Fig. 10 Case P2, NPP ratio 128:64. Convergence of C_L at $\alpha = 1.5°$ and $M = 0.75$.

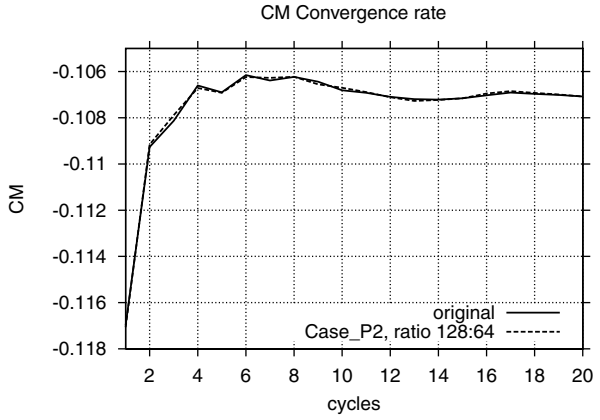

Fig. 11 Case P2, NPP ratio 128:64. Convergence of C_M at $\alpha = 1.5°$, $M = 0.75$.

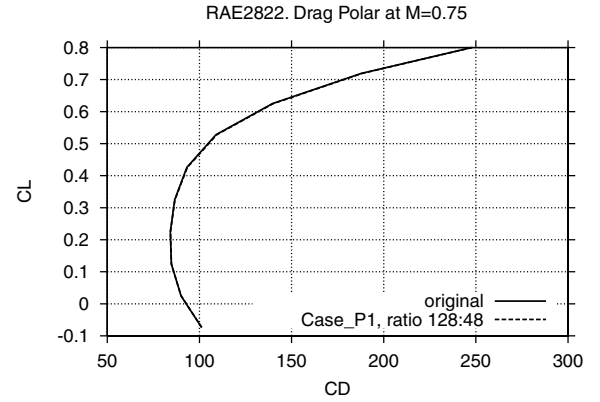

Fig. 12 Drag polar at $M = 0.75$ fr case P1, NPP ratio 128:48 vs original point-to-point case.

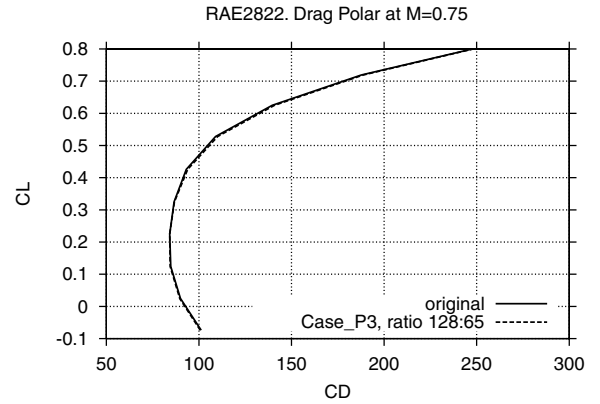

Fig. 13 Drag polar at $M = 0.75$ for case P3, NPP ratio 128:64 vs original point-to-point case.

(case P4). Note that in case P3–case P4, the relevant interblock boundary intersects the supersonic zone in the considered transonic flight conditions.

The grid details can be found in Figs. 3–5, in which iso-Mach contours for different test cases are presented. As can be seen from these figures, the flow structure is basically independent on the location of the nonmatched grid line.

Even in case P3 (Fig. 4), in which the nonmatched boundary intersects the supersonic bell, iso-Mach contours are very similar to those in less challenging case P1 and case P2. In the most challenging case, case P4, in which the above nonmatched boundary is very close to the airfoil surface the numerical simulation yields less smooth contours. Still away from the surface boundary there was limited

Table 2 Block dimensions of the first point-to-point mesh around the three-dimensional wing

Index	nf_wing blocks	nf_wake blocks	ff_wing blocks	ff_wake blocks
i_{max}	128	32	128	32
j_{max}	28	28	12	12
k_{max}	36	36	36	36

Table 3 List of test cases for flow over a 3-D generic wing

Blocks total	Blocks modified	Axes modified	New dimensions	Original dimensions
		Case 3DW1		
8	ff_up_wing	*i*	64	128
		Case 3DW2		
8	ff_up_wing	*i*	48	128
		Case 3DW3		
16	ff_up_wing	*i*	48	128
16	ff_up_wing	*j*	24	12
		Case 3DW4		
16	ff_up_wing	*i*	64	128
16	ff_up_wing	*j*	24	12
16	ff_lo_wake	*i*	20	32
		Case 3DW5		
16	ff_up_wing	*i*	48	128
16	ff_up_wing	*j*	24	12
16	ff_lo_wake	*i*	20	32
		Case 3DW6		
16	ff_up_wing	*i*	48	128
16	ff_up_wing	*j*	24	12
16	ff_up_wing	*k*	40	20
16	ff_lo_wake	*i*	20	32

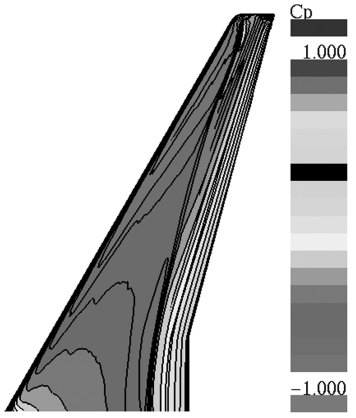

Fig. 14 Flow over a generic 3-D wing with original point-to-point mesh and pressure distribution on the upper wing surface at $M = 0.80$ and $\alpha = 1.5°$.

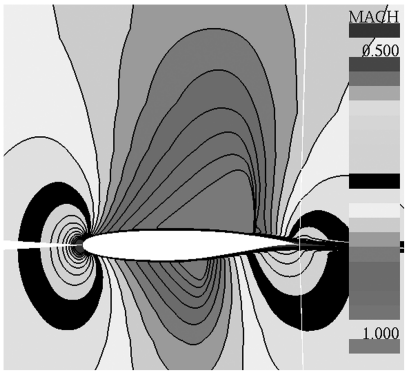

Fig. 15 Flow over a generic 3-D wing with original point-to-point mesh and iso-Mach contours in the symmetry plane at $M = 0.80$ and $\alpha = 1.5°$.

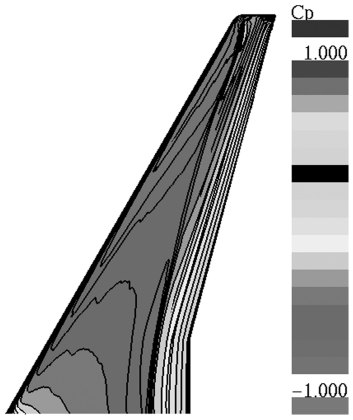

Fig. 16 Flow over a generic 3-D wing for case 3DW1 and pressure distribution on the upper wing surface at $M = 0.80$ and $\alpha = 1.5°$.

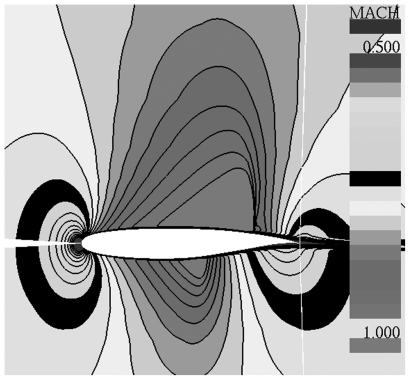

Fig. 17 Flow over a generic 3-D wing for case 3DW1 and iso-Mach contours in the symmetry plane at $M = 0.80$ and $\alpha = 1.5°$.

observed differences in the flowfield and the numerical noise is confined to the vicinity of the interblock boundary.

The pressure distributions corresponding to case P3–case P4 are presented in Figs. 6–8 in comparison with the original point-to-point case. In case P2 the two distributions are practically identical. The same is also true for case P3, NPP ratio 128:64 (Fig. 6). Note that C_P distribution in case P3, NPP ratio 128:48 (Fig. 7), is almost unaffected by the nonsmooth tailoring of the corresponding NPP boundary. Even in case P4 (Fig. 8) the NPP numerical simulation yielded the surface pressure distribution very close to the original one, though the source of numerical noise is very close to the airfoil surface.

In all the above numerical simulations, the computational process preserves the convergence and numerical stability of the original single-grid computation for the problem considered here. To illustrate this, the convergence history of major aerodynamic characteristics (drag coefficient C_D, lift coefficient C_L and pitching moment C_M) is presented in Figs. 9–11, respectively, for case P2, NPP ratio 128:64, in comparison with the original point-to-point case. It can be concluded that the convergence properties were unaffected by the introduction of NPP boundary, and that the integral aerodynamic characteristics correlate well with the original values. The last statement stays correct in the wide range of flight conditions, which is demonstrated in Figs. 12 and 13, in which the drag polars for different NPP cases are depicted.

As a test case for three-dimensional verification of the method, a generic-jet-type wing was chosen. The flow over the wing is highly-three-dimensional in transonic flight conditions, due to its glovelike planform and supercritical wing sections.

Two original point-to-point meshes with C-O topology were considered. The first grid comprised eight blocks. The near-field group of blocks included four blocks (upper wing, lower wing, upper wake and lower wake), and the far-field group included the corresponding extension of the near-field blocks in the direction of the computational infinity. In all the blocks indices i, j and k were oriented along streamwise, normal to the wing surface and spanwise directions, respectively. The dimensions of the blocks are given in Table 2. The total number of cells was equal to 460,800.

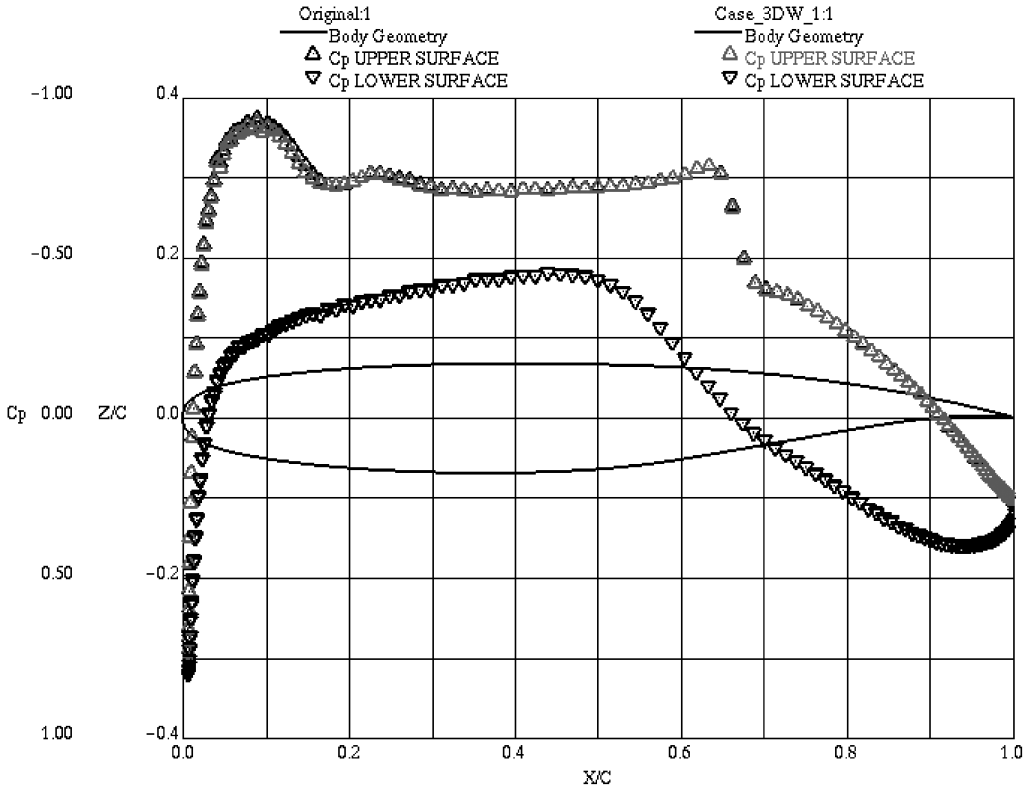

Fig. 18 Flow over a generic 3-D wing for point-to-point case vs case 3DW1 at $M = 0.80$ and $\alpha = 1.5°$; sectional C_P is at midwing.

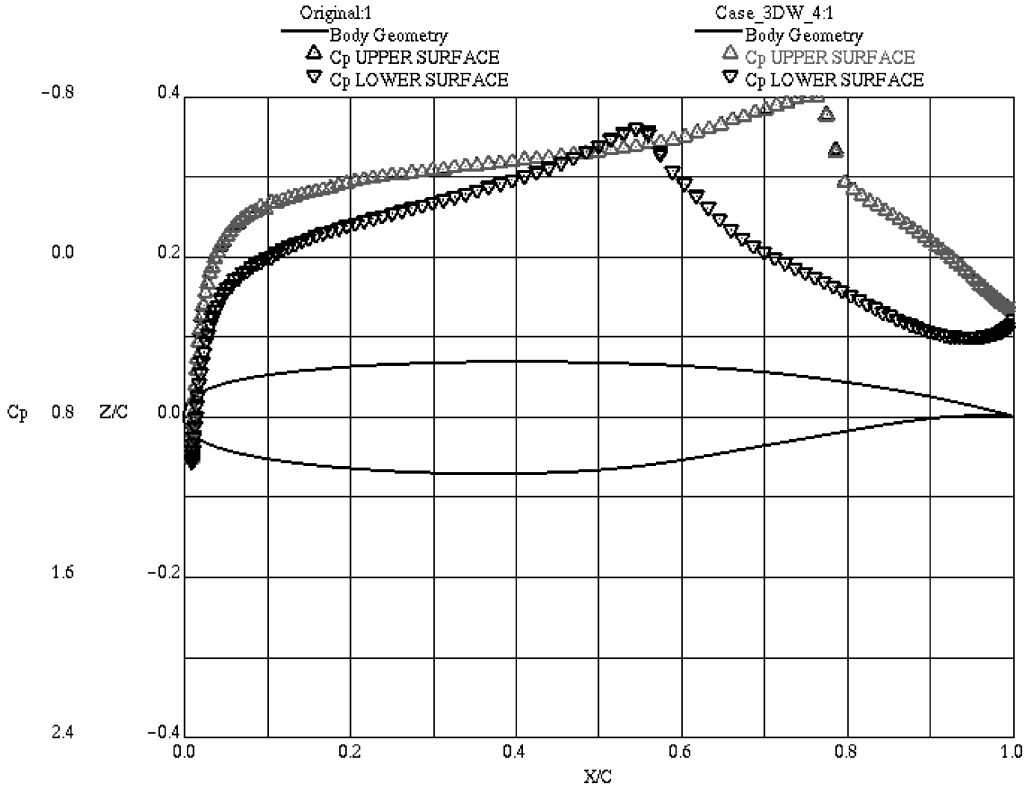

Fig. 19 Flow over a generic 3-D wing for point-to-point case vs case 3DW4 at $M = 0.80$ and $\alpha = 1.5°$; sectional C_P is at the symmetry plane.

The second mesh was constructed by additionally dividing the blocks of the first mesh in the span direction (index k) with the purpose to allow for various locations of NPP boundaries. In the second mesh, the dimensions of all the blocks in the i and j directions remained unchanged, whereas the value of $k_{\max} = 20$ for the first eight inboard blocks and $k_{\max} = 16$ for the last eight outboard blocks.

In total, six test cases were considered (labeled case 3DW1 to case 3DW6). The meshes of the test cases with non-point-to-point-matched block boundaries were constructed by changing the dimensions of one or more original blocks in some of the directions i, j, k. Thus, the test cases differ in the number of modified original blocks and the number of modified directions in the blocks. The corresponding data are presented in Table 3.

The verification of the proposed method was performed at the following cruise flight conditions: $M = 0.80$, $Re = 4.7 \cdot 10^6$, and $\alpha = 1.5°$. First, we present the results corresponding to the original point-to-point mesh. The computations yielded $C_L = 0.4935$, $C_D = 201.8$ aerodynamic counts. The pressure distribution on the upper surface of the wing related to this computation is given in Fig. 14, and the iso-Mach contours at the symmetry plane are presented in Fig. 15. We can see that the flow developed a strong three-dimensional λ-type shock.

The first test case (case 3DW1) deals with one nonmatched interblock face with ratio 64:128 in the streamwise direction. The corresponding data are presented in Figs. 16–18, in which C_P distribution on the upper wing surface, iso-Mach contours at the symmetry plane, and sectional pressure distributions at midsection of the wing, respectively, are depicted. The comparison with the original point-to-point computation shows that the introduction of NPP face had almost no impact on the resulting flowfield, and the two surface pressure distributions are practically identical. This is also true in terms of major aerodynamic coefficients and moments.

The second test case (case 3DW2) differs from the previous one by the resolution in the modified block with NPP ratio 48:128, which models arbitrary partition. Nevertheless the mesh coarsening did not change the accuracy of computations.

The next four test cases deal with 16-block grid topology and essentially higher diversity of locations, directions, and NPP ratios for the nonmatched interblock boundaries.

In total, in cases 3DW4–3DW5, there are six nonmatched faces: four NPP faces in the far-field upper wing block and two NPP faces in the far-field low-wake block. Five NPP faces contain only one nonmatched direction, whereas the remaining NPP face is nonmatched in the both face directions. The corresponding NPP ratios may be found in Table 3. Note that in the both cases the resolution of the first NPP block (upper wing) was increased in the $j$direction, whereas it was decreased in the i direction. The corresponding data are presented in Figs. 19 and 20. It can be seen that similar to the previous cases, the flow structure remained unchanged, including sensitive sectional surface C_P distributions.

Finally, let us consider the last, most challenging, case: case 3DW6, in which all NPP faces of the first modified block were nonmatched in the both directions. Though here a little bit more distinctions exist between NPP results and point-to-point computations, the accuracy is still kept to a reasonably high level. This is illustrated by Fig. 21, in which surface pressure at the midwing section is given. At the root section the point-to-point and NPP computations yield almost identical distributions, whereas at the midwing section, a minor discrepancy may be observed.

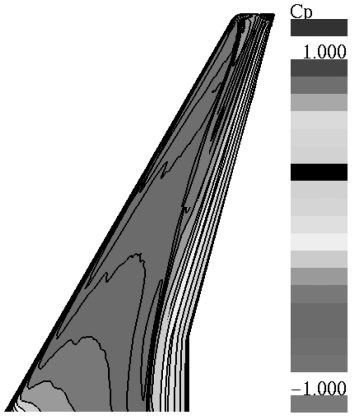

Fig. 20 Flow over a generic 3-D wing for case 3DW5 pressure distribution on the upper wing surface at $M = 0.80$, $\alpha = 1.5°$.

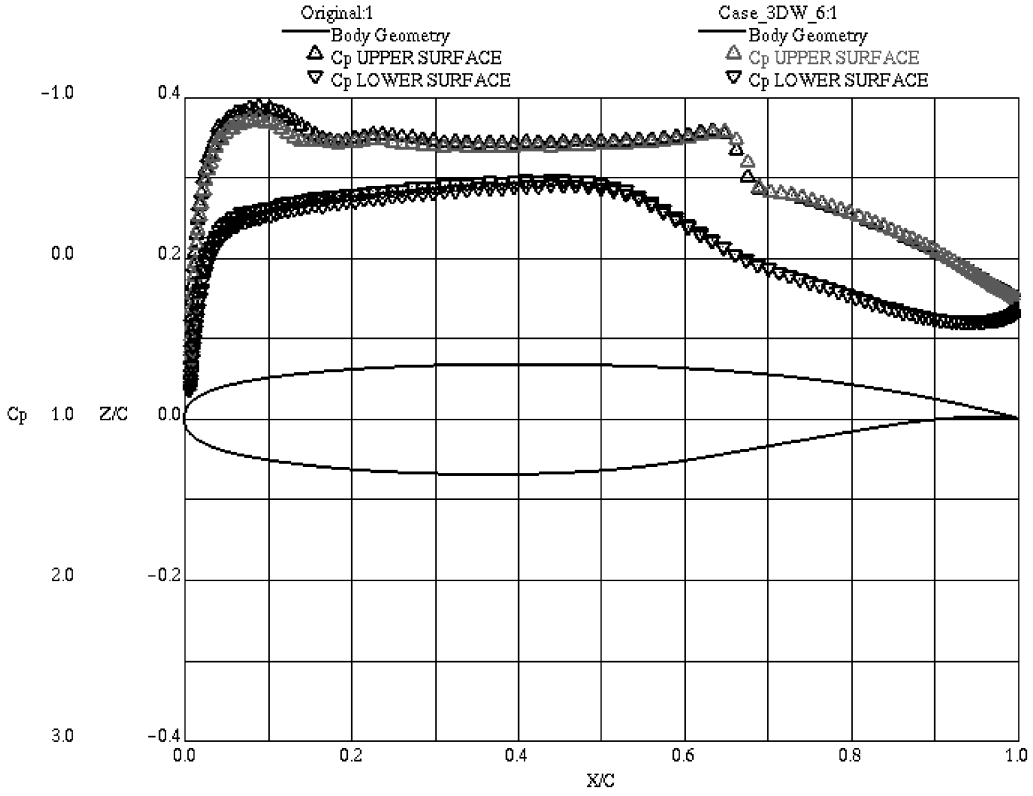

Fig. 21 Flow over a generic 3-D wing for point-to-point case vs case 3DW6 at $M = 0.80$ and $\alpha = 1.5°$; sectional C_P at the midwing.

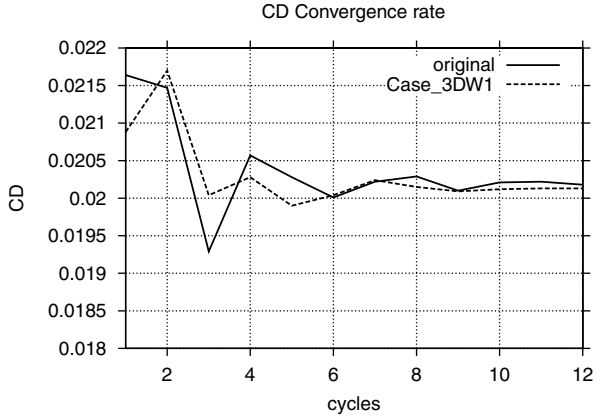

Fig. 22 Flow over a generic 3-D wing for case 3DW1. Convergence of C_D at $\alpha = 1.5°$ and $M = 0.80$.

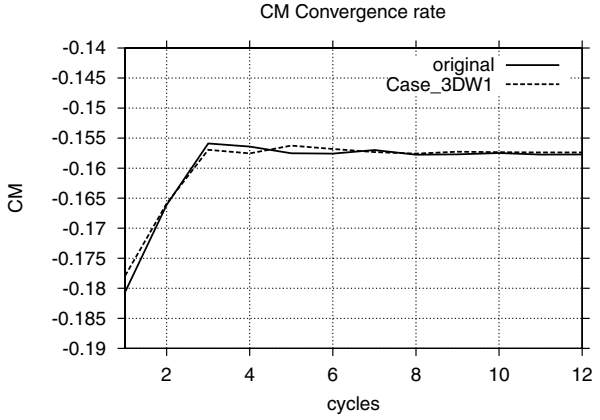

Fig. 23 Flow over a generic 3-D wing for case 3DW1. Convergence of C_M at $\alpha = 1.5°$ and $M = 0.80$.

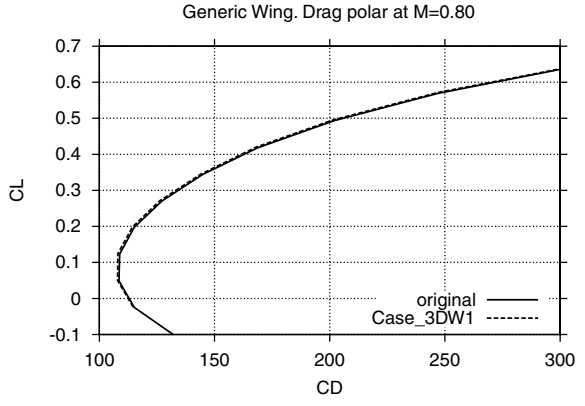

Fig. 24 Flow over a generic 3-D wing. Drag polar at $M = 0.80$. Point-to-point case vs case 3DW1. case.

Similar to 2-D test cases, the computational process preserves the convergence and numerical stability of the original single-grid computation for the problem considered here. The corresponding data can be found in Figs. 22 and 23, in which the convergence history of major aerodynamic characteristics (drag coefficient C_D and pitching moment C_M) is presented for case 3DW1 in comparison with the point-to-point computations. It can be concluded that the proposed method of treating nonmatched interblock boundaries preserves good convergence and numerical stability properties, exhibited by the original point-to-point computations. Additionally, the NPP approach as implemented compares well with the original point-to-point approach for force and moment computations on the problems considered here, which is illustrated in Fig. 24, in which the drag polars for case 3DW1 are depicted.

VI. Conclusions

A new approach to the treatment of non-point-to-point structured grids for the solution of full Navier–Stokes equations is proposed.

The approach was implemented within the framework of a high-accuracy finite volume scheme. The method introduces narrow cell clusters located in the vicinity of interblock nonmatched boundaries, in which the computational fluxes are directly optimized. The constraints placed upon the optimum ensured flux conservative property. The computational results, which included a number of transonic numerical test cases for realistic aerodynamic configurations, indicate robustness and good engineering accuracy of the method.

References

[1] Peigin, S., Epstein, B., Rubin, T., and Seror, S., "Parallel Large Scale High Accuracy Navier–Stokes Computations on Distributed Memory Clusters," *Journal of Supercomputing*, Vol. 27, No. 1, Jan. 2004, pp. 49–68. doi:10.1023/A:1026246805774

[2] Rai, M. M., "Conservative Treatment of Zonal Boundaries for Euler Equation Calculations," *Journal of Computational Physics*, Vol. 62, No. 2, 1986, pp. 472–503. doi:10.1016/0021-9991(86)90141-5

[3] Bohbot, J., Jouhaud, J. C., and Darracq, D., "Coupled Patched-Grid AMR Meshing Techniques for Transonic Aircraft Design," AIAA Paper 2002-0546.

[4] Chen, H. X., and Fu, S. J., "Navier–Stokes Simulations for Transport Aircraft Wing-Body Combinations with Deployed High-Lift Systems," AIAA Paper 2003-4077, 2003.

[5] Chen, S., Khalid, M., and Zhang, S., "A Non-Contiguous Grid Generation Method Using ICEMCFD's HEXA," *9th Annual Conference of the CFD Society of Canada*, Waterloo, Canada, May 2001, pp. 143–151.

[6] Nataf, F., and Rogier, F., "Factorization of Convective-Diffusion Operator and the Schwarz Algorithm," *Mathematical Models and Methods in Applied Sciences*, Vol. 5, No. 1, 1995, pp. 67–93. doi:10.1142/S021820259500005X

[7] Berger, M., and LeVeque, R., "A rotated Scheme for Cartesian Grids in Complex Geometries," AIAA TR CP-91-1602, 1991.

[8] Epstein, B., Luntz, A., and Nachshon, A., "Multigrid Euler Solver about Arbitrary Aircraft Configurations with Cartesian Grids and Local Refinements," AIAA Paper 1989-1960, 1989.

[9] Epstein, B., Averbuch, A., and Yavneh, I., "An Accurate ENO Driven Multigrid Method Applied to 3-D Turbulent Transonic Flows," *Journal of Computational Physics*, Vol. 168, No. 2, 2001, pp. 316–338. doi:10.1006/jcph.2001.6698

[10] Epstein, B., Rubin, T., and Seror, S., "Accurate Multiblock Navier–Stokes Solver for Complex Aerodynamic Configurations," *AIAA Journal*, Vol. 41, No. 4, 2003, pp. 582–594. doi:10.2514/2.2012

[11] Shu, C.-W., Zang, T. A., Erlebacher, G., Whitaker, D., and Osher, S., "High-Order ENO Schemes Applied to Two- and Three-Dimensional Compressible Flow," Institute for Computer Applications in Science and Engineering Rept. 91-38, Hampton, VA, 1991.

[12] Harten, A., Engquist, B., Osher, S., and Chakravarthy. S., "Uniformly High Order Accurate Non-Oscillatory Schemes. 1," *Journal of Computational Physics*, Vol. 71, No. 2, 1987, pp. 231–303. doi:10.1016/0021-9991(87)90031-3

[13] Shu, C.-W., and Osher, S., "Efficient Implementation of Essentially Non-Oscillatory Shock-Capturing Schemes," *Journal of Computational Physics*, Vol. 83, No. 1, 1989, pp. 32–78. doi:10.1016/0021-9991(89)90222-2

[14] Epstein, B., and Nachshon, A., "An ENO Navier–Stokes Solver Applied to 2-D Subsonic, Transonic and Hypersonic Aerodynamic Flows," AIAA Paper 94-0303, 1994.

[15] Rome, C., "A Connecting Method of Block-Structured Meshes for Resolution of Navier–Stokes Equations," Ph.D. Thesis, Univ. of Bordeaux I, Bordeaux, France, 2006.

[16] Bourisli, R., and Kaminski, D., "Evolutionary Optimization Techniques as Versatile Solvers for Hard-to-converge Problems in Computational Fluid Dynamics," *International Journal for Numerical Methods in Fluids*, Vol. 52, No. 3, 2006, pp. 321–354. doi:10.1002/fld.1184

[17] Bunning, P. G., Jespersen, D. C., Pulliam, T. H., Chan, W. M., Stomock, J. P., Krist, S. E., and Renze, K. I., "OVERFLOW User's Manual, Ver. 1.81," NASA Langley Research Center, Hampton, VA, 1999.

[18] Epstein, B., Jameson, A., Peigin, S., Roman, D., Harrison, N., and Vassberg, J., "Comparative Study of Three-Dimensional Wing Drag Minimization by Different Optimization Techniques," *Journal of Aircraft*, Vol. 46, No. 2, 2009, pp. 526–541. doi:10.2514/1.38216

Z. Wang
Associate Editor